Silica Crystalline Colloidal Array Deep Ultraviolet Narrow-Band Diffraction Devices

LULING WANG, ALEXANDER TIKHONOV, and SANFORD A. ASHER*

Department of Chemistry, University of Pittsburgh, Pittsburgh, Pennsylvania 15260

We developed a facile method to fabricate deep ultraviolet (UV) photonic crystal crystalline colloidal array (CCA) Bragg diffraction devices. The CCAs were prepared through the self-assembly of small, monodisperse, highly surface charged silica particles (~50 nm diameter) that were synthesized by using a modified Stöber process. The particle surfaces were charged by functionalizing them with the strong acid, non-UV absorbing silane coupling agent 3-(trihydroxylsilyl)-1-propane-sulfonic acid (THOPS). These highly charged, monodisperse silica particles self assemble into a face-centered cubic CCA that efficiently Bragg diffracts light in the deep UV. The diffracted wavelength was varied between 237 nm to 227 nm by tilting the CCA orientation relative to the incident beam between glancing angles from 90° to ~66°. Theoretical calculations predict that the silica CCA diffraction will have a full width at half-maximum (FWHM) of 2 nm with a transmission of $\sim 10^{-11}$ at the band center. We demonstrate the utility of this silica CCA filter to reject the Rayleigh scattering in 229 nm deep UV Raman measurements of highly scattering Teflon.

Index Headings: **Wavelength-selective optical devices; UV Raman spectroscopy; Narrow band diffraction; Silica crystalline colloidal array; CCA.**

INTRODUCTION

The development of novel wavelength-selective optical devices enables major advances in spectroscopic methodologies and instrumentation.[1–16] Spectroscopies such as Raman, fluorescence, hyperspectral imaging, and pump-probe techniques require wavelength-selective optical elements that reject particular regions of the electromagnetic spectrum while transmitting adjacent spectral regions.[5–8,10,11,17] The recent development of highly efficient holographic filters and multilayer dielectric filters has dramatically advanced near ultraviolet (UV), visible, and near-infrared (NIR) spectroscopies.[9–12,18–21] Unfortunately, analogous devices do not exist in the deep UV because the typical materials used absorb deep UV light.[9,22,23] Thus, the important new field of deep UV Raman spectroscopy has not benefited from these instrumentation advances.

In the mid-1980s we developed the first photonic crystal device.[7,8,15,16] This optical device, which functioned as a Bragg diffraction filter, was fabricated from a crystalline colloidal array (CCA) of ~100 nm diameter highly charged, monodisperse polystyrene particles.[7,8] These highly charged particles self assembled into a face-centered cubic structure that efficiently Bragg diffracted light from its 111 planes but freely transmitted light in adjacent spectral regions. This optic functioned as a highly efficient Rayleigh rejection filter for Raman measurements. This device was licensed from the University of Pittsburgh by EG&G Princeton Applied Research and was commercialized. These CCA Rayleigh rejection filters also served as the basis of novel Raman spectrometers.[7,8,15,16] This CCA technology was leapfrogged in the 1990s when holographic filters became readily available.[24–26]

In the work here we describe an analogous photonic crystal device that functions as an efficient Bragg diffraction filter in the deep UV. To accomplish this we developed a method to prepare CCA photonic crystals of silica spheres that efficiently diffract but do not absorb deep UV light.[7,8,22,27,28] To accomplish this we developed a facile method to fabricate ~50 nm diameter monodisperse, highly charged silica particles that self assemble into CCAs. We also here demonstrate the utility of this highly charged silica CCA as a Rayleigh rejection filter in deep UV Raman measurements.[28]

EXPERIMENTAL

Fabrication of Highly Charged, Monodisperse, Small Silica Particles. We synthesized monodisperse, small silica particles by using a modified Stöber method.[29] We then functionalized the silica particle surface with a low deep UV absorption silane coupling agent (3-(trihydroxylsilyl)-1-propane-sulfonic acid (THOPS, 30% in water, Gelest, Inc.). A typical reaction used 5 mL tetraethoxysilane (TEOS, Fluka, Lot code 133281541207016) as the silica precursor, 8 mL ammonium hydroxide (29.40 wt%, J. T. Baker) as the catalyst, and 200 mL ethanol as the reaction solvent. The reaction mixture was stirred for 24 h. The resulting silica dispersion was filtered through nylon mesh (Small Parts, Inc). Then, 200 mL of water was slowly added to the Stöber silica dispersion under stirring. The mixture was first heated to 50 °C for ~30 min, then heated to 80 °C for ~1 h. Six milliliters (6 mL) of the silane coupling agent THOPS was adjusted to pH ~6 with ammonium hydroxide and then added to the silica dispersion. The reaction was refluxed for 6 h at 80 °C.

Silica CCA Fabrication and Transmission Measurements. The functionalized silica colloids were cleaned by six repetitions of centrifugation at 12 000 rpm and redispersion of the resulting silica pellet in Nanopure water (Barnstead). The silica particle concentration was adjusted by controlling the amount of water added during the last redispersion. Further purification was achieved by shaking the silica dispersion with mixed bed ion-exchange resin (Bio-Rad AG 501-X8). After purification, these highly charged silica particles self assemble into CCA at volume concentrations above 1%. The surface charge density of the functionalized silica particles was determined by conductrometric titration (712 conductometer, Brinkmann and 794 Basic Titrino, Metrohm) with 0.01 N standard NaOH solutions (Fisher Scientific Inc.).

The CCA filter cell is shown in Fig. 1a. Two fused silica quartz discs (2″ dia. × 3/16″) were separated by a ~125 μm

Received 9 November 2012; accepted 21 December 2012.
* Author to whom correspondence should be sent. E-mail: asher@pitt.edu.
DOI: 10.1366/11-06527

0003-7028/12/6604-0426$2.00/0

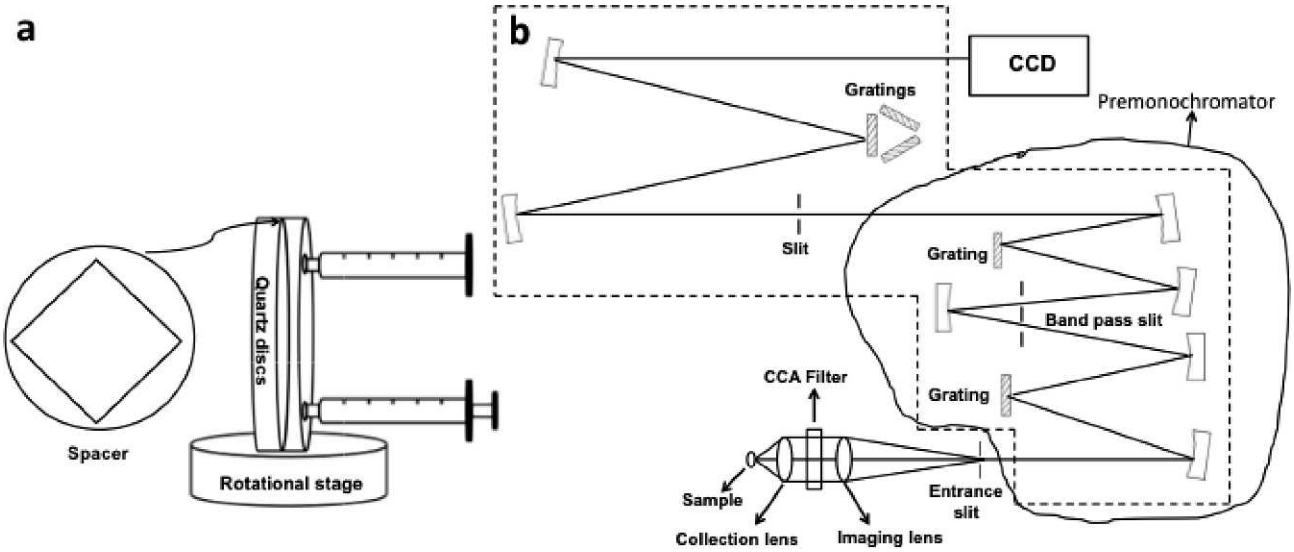

FIG. 1. (**a**) A CCA flow cell for transmission measurements; (**b**) schematic of triple-stage monochromator for Raman measurements.

thick Parafilm spacer and mounted on a rotation stage. The highly charged silica colloidal dispersion (volume percent 7.0%) was carefully injected into one of the holes in one of the quartz discs to fill the cell, in order to avoid bubbles. The system self assembled into a CCA. Transmission spectra of the CCA filter with incident glancing angles at 90°, 69°, and 66° were measured with a Cary 5000 (Varian, Inc.) spectrophotometer using the double beam mode and zero/baseline correction.

Silica CCA Rayleigh Rejection Filter Raman Measurements. We measured deep UV Raman spectra of highly scattering Teflon with excitation at the 229 nm line (2 mW) by using a continuous-wave UV Ar laser (Innova 300 FReD, Coherent, Inc.). The laser excited the Teflon sample in a backscattering geometry with the laser beam focused to a ~20 μm diameter spot. Figure 1b shows the schematic of the triplemate monochromator used for the Raman measurements.

The spectrometer filter stage premonochromator was aligned to conveniently block a portion of the Rayleigh scattered light to allow us to make quantitative measurements of the CCA laser light attenuation. The spectrometer setups were identical for Raman spectra measured in the absence and presence of the CCA filter. The CCA filter was placed between a collection and imaging lens (Fig. 1b) where the light is collimated.

Characterization Techniques. We measured the silica particle sizes by using dynamic light scattering (DLS) and transmission electron microscopy (TEM). DLS and zeta potential were measured by using a Brookhaven Instruments Corporation ZetaPALS. The silica particles were also examined by using a JEOL 200 CX TEM. A few drops of the dilute silica particle dispersion were dried on a carbon-coated copper grid (Ted Pella, Inc.) for the TEM measurements.

RESULTS AND DISCUSSION

Fabrication of Highly Charged, Monodisperse, Small Silica Particles. We used a modified Stöber method to prepare the Stöber silica dispersion in which an aqueous ammonium hydroxide solution is used instead of saturated alcoholic solutions of ammonia.[29] The typical recipe yielded Stöber silica particles with a diameter of 53.6 ± 0.3 nm (polydispersity 0.045) as determined by DLS. Figure 2a shows a TEM image of monodisperse silica particles with a diameter of 43.6 ± 3.9 nm. The TEM diameter is smaller than that measured by DLS because DLS measures the hydrodynamic diameter while TEM measures the diameter of the dehydrated particles.

The Stöber silica dispersion after cleaning and ion-exchange does not have sufficient surface charge to self assemble into CCA; the pK_a of the surface –SiOH is relatively high (~7.1).[30] The zeta potential of these cleaned Stöber silica particles is only −12 mV at pH 4.0. We developed a facile method to attach strong sulfonic acid groups ($–SO_3H$) to the surface of the monodisperse silica colloids by using THOPS as the silane coupling agent. THOPS was attached to the silica particle surface by a condensation reaction between the silanols (–SiOH) groups on the Stöber silica surface and that of THOPS. The resulting silica particles are highly charged due to the low pK_a of < 1 of the surface sulfonic acid groups.[31] Because the Stöber silica dispersion is only stable at basic pH,[32] we found that the silica particles immediately aggregate if we directly added the THOPS solution (pH = 0.34) to the Stöber silica dispersion. However, aggregation does not occur if we adjust the THOPS pH to ~6 before addition. After cleaning and ion exchange, the surface functionalized silica particles self assemble into CCA.

Figure 2b shows a TEM image of our charged silica CCA particles, which show an average diameter of 47.3 ± 5.1 nm. The diameter measured by DLS is 60.2 ± 0.3 nm, slightly larger than that determined by TEM. The zeta potential of the charged silica particles is −43 mV (pH 4.0), which indicates high surface charge. We also determined the surface charges of these silica CCA particles by using conductometric titration with 0.01 N NaOH. The typical recipe yields 4740 charges per silica particle (10.8 $\mu C/cm^2$). Table I shows that the surface charge density of the silica particles can be easily tuned by varying the amount of THOPS during the surface modification. The zeta potential increases as we increase the amount of THOPS during the surface modification reaction.

Although our main objective here is to fabricate highly charged, monodisperse silica particles with diameters ~50 nm, we were also able to prepare highly charged larger silica particles. The silica particle size strongly depends on the

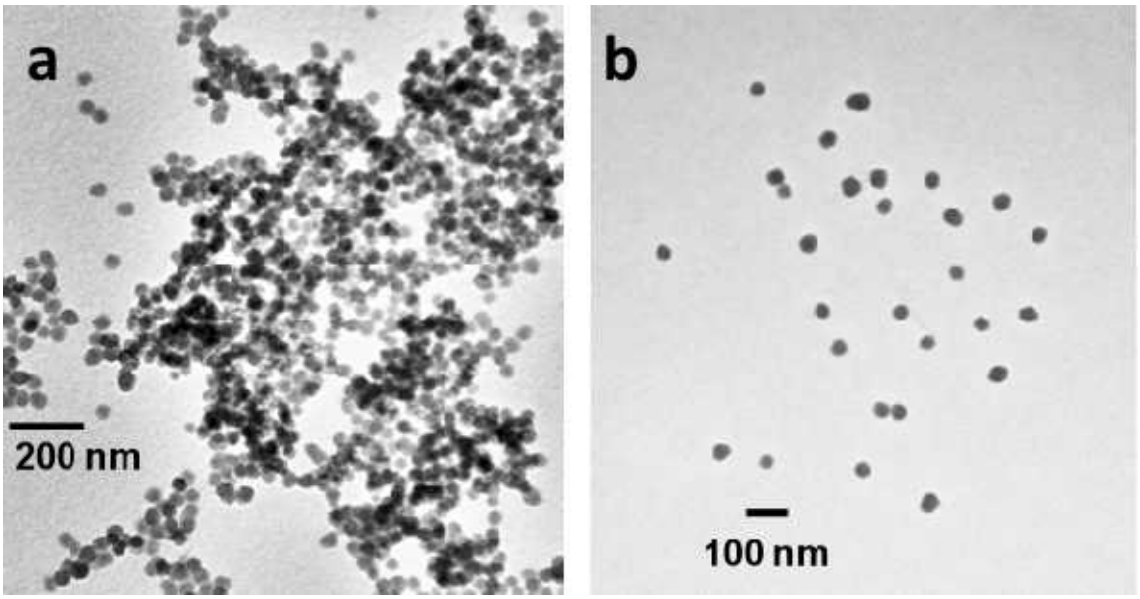

FIG. 2. TEM images of (**a**) the Stöber silica particles; (**b**) our surface functionalized silica particles.

amount of ammonium hydroxide added during the Stöber silica condensation process.[29] Figure 3 shows the TEM images of highly charged silica CCA with an average diameter of (a) 70 ± 5 nm and (b) 237 ± 7 nm. The zeta potentials for these two samples are (a) −33 mV and (b) −46.7 mV, respectively, indicating that the silica particles are highly charged.

Transmission Measurements of Silica CCA. The highly charged silica particles self assemble into a CCA after cleaning and ion exchange. The silica CCA diffraction wavelength can be calculated from Bragg's and Snell's laws according to Eqs. 1 and 2, where λ_0 is the wavelength in air diffracted by the CCA, which depends on the average refractive index of the CCA, n_{avg}, the lattice spacing, d, and the incident light glancing angle, θ. The glancing angle, θ, in the CCA medium is calculated from Snell's law for refraction, where θ_0 is the incident glancing angle in air.[27,33–35]

$$\lambda_0 = 2n_{avg}d\sin\theta \tag{1}$$

$$\theta = \cos^{-1}\left[\frac{\cos\theta_0}{n_{avg}}\right] \tag{2}$$

According to Bragg's law, the CCA diffracted wavelength, λ_0, can be easily tuned by adjusting the filter orientation relative to the incident light (θ_0). Larger diffraction wavelength shifts are obtained by changing the particle spacing by adjusting the concentrations of the CCA particles. We diluted the concentrated highly charged silica particles after the last centrifugation to obtain a volume concentration of 6–7%, for which the silica CCA dispersion Bragg diffracts light in the deep UV. The concentration of the silica CCA was determined gravimetrically from the ratio of the dry weight of the silica CCA particles to the overall weight of the silica CCA dispersion.

The silica CCA dispersion is visually transparent because only light in the deep UV range is diffracted. Figure 4 shows transmission spectra of the silica CCA (volume percent 7.0%) for incident glancing angles of 90°, 69°, and 66°. The band rejection wavelength was tuned from 237 nm, to 229 nm, and to 227 nm by tilting the filter with respect to the incident beam from 90°, to 69°, and to 66°, as shown in Fig. 4. The bandwidths determined from these transmission measurements are broader than the true CCA bandwidths because the absorption spectrophotometer utilizes a somewhat focused exciting beam. The measured attenuation is also artifactually decreased. For normal incidence in Fig. 4 the full bandwidth at half-maximum (FWHM) observed is 5.0 nm. The CCA filter shows only slight broadening of the rejected FWHM as the filter is angle-tuned, with a FWHM of 5.9 nm as the incident glancing angle is tuned to 69° and 66°. The diffraction efficiency will decrease for the π polarization as the incident beam is tuned away from the normal to the crystal plane.[36] The effective half bandwidth should increase for the π polarization relative to the σ polarization for perfectly collimated light.[36] The small changes observed clearly indicate that the spectral bandwidth is dominated here by the CCA disorder and/or the lack of incident collimation.

The lattice spacing d of the CCA depends on the silica CCA particle diameter, particle volume concentration, and the CCA photonic crystal structure (face-centered cubic (FCC) or body-centered cubic (BCC) structure). From the lattice spacing, we

TABLE I. Dependence of silica CCA particle surface charge on THOPS.[a]

Sample	Diameter/nm (TEM)	THOPS/mL	Charges per particle	Charge density (μC/cm^2)	Zeta potential (mV)
A	46.1 ± 5.7	2	1094	2.6	−31
B	48.8 ± 5.1	4	2847	6.1	−40
C	47.3 ± 5.1	6	4736	10.8	−43

[a] Only the amount of THOPS is varied, with the other conditions remaining that of the typical recipe.

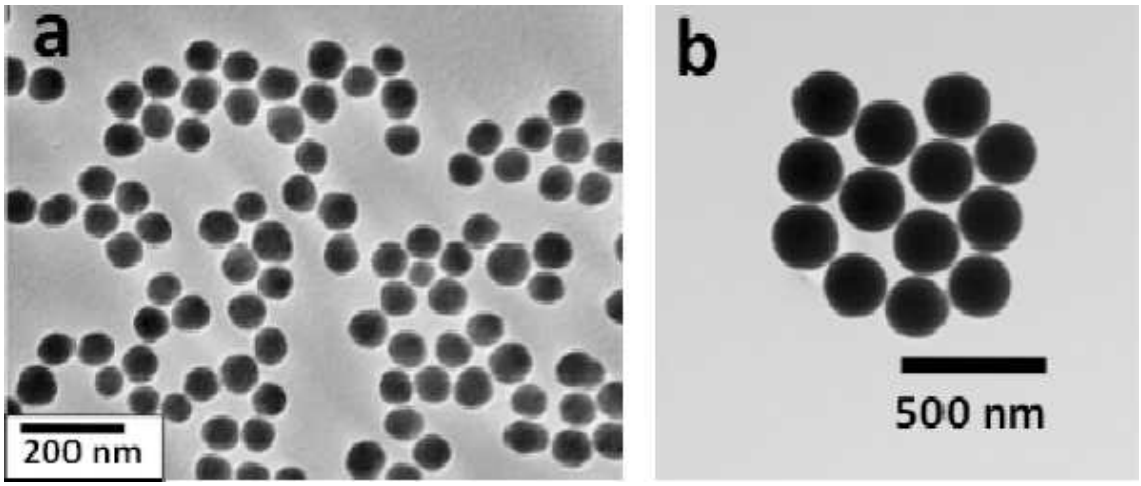

FIG. 3. TEM images of samples (**a**) synthesized with 10 mL and (**b**) 15 mL of ammonium hydroxide in the Stöber silica synthesis. 2 mL of THOPS was added in the surface modification. Other conditions are those of the typical recipe.

can easily calculate the diffracted wavelength by using Eqs. 1 and 2. For silica CCA particles with a diameter of 47.3 nm and a volume percentage of 7%, we calculate the diffracted wavelength at the normal incidence to be 236.6 nm for the FCC (111) diffraction and 230.0 nm for the BCC (110) diffraction. Our transmission measurements (Fig. 4) show a diffracted wavelength of 237 nm at the normal incidence, indicating the silica CCA has a FCC structure.

The width of the narrow wavelength Bragg diffraction band depends on the degree of ordering of the silica FCC array within the CCA, the particle diameter, the CCA thickness, and the difference between the refractive indices of the charged silica particles and the medium.[8,27,37,38] The diffraction was theoretically calculated by modeling the 3D CCA FCC (111) layers as a 1D stack of dielectric slabs.[27,37,39]

Figure 5 compares the observed and calculated diffraction of this silica CCA filter. The dashed line shows the observed light diffraction transmission of the CCA dispersion relative to that of the cell filled with water as obtained in Fig. 4. The solid line shows the calculated diffraction from a silica CCA consisting of 1200 FCC (111) silica particle layers (101 μm total thickness, silica particle diameter of 47.3 nm). Theory predicts a FWHM of 2 nm and an ultra high attenuation Bragg diffraction transmission of $\sim 10^{-11}$ at 237 nm. The difference between the observed and theoretical results is presumably due to crystal disorder in the CCA.[38]

Utilization of CCA for UV Raman Rayleigh Rejection. The highly charged silica CCA of Fig. 4 was used to reject Rayleigh scattered light in 229 nm excited Raman measurements of Teflon. To conveniently avoid saturating the CCD camera and to quantitatively measure the CCA filter rejection efficiency, we carefully adjusted the premonochromator shown in the Fig. 1b so that it blocked a portion of the Rayleigh scattered light. The CCA filter was placed between the collection and imaging lens (Fig. 1b) where the light is collimated.

Figure 6 shows that the Teflon Raman spectrum measured in the absence of the CCA filter shows a high "Rayleigh peak." The Fig. 6 Teflon Raman spectrum measured using the CCA filter at an incident glancing angle of ~69° shows a dramatically decreased Rayleigh scattering because the CCA filter Bragg diffracts 229 nm light at the ~69° incident angle orientation (Fig. 4). Figure 6 indicates that the CCA filter (at the incident glancing angle of ~69°) rejects 99.82% (ratio of

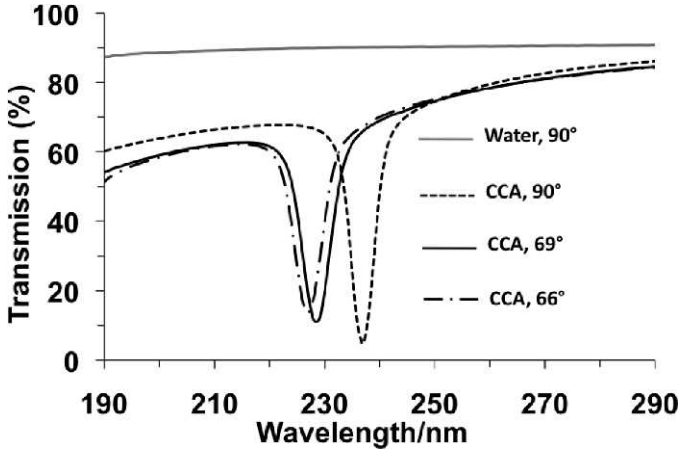

FIG. 4. Transmission spectra of a flow cell filled with pure water and of the flow cells filled with highly charged silica CCA dispersion for incident glancing angles of 90°, 69°, and 66°. Silica colloid diameter is 47.3 ± 5.1 nm.

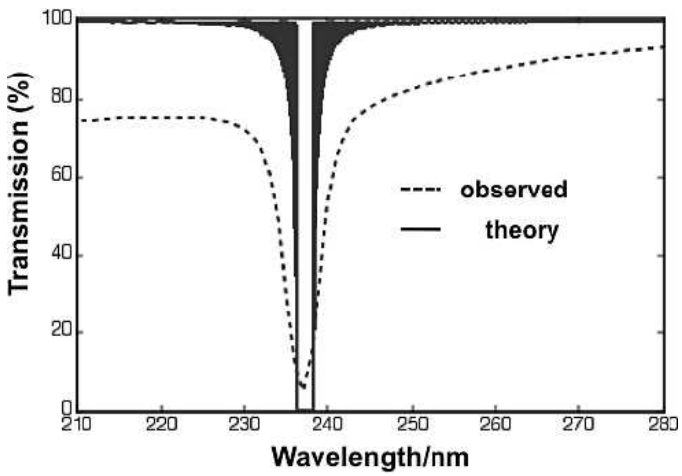

FIG. 5. Observed and calculated transmission spectrum of diffraction by silica CCA at a 90° incident angle.

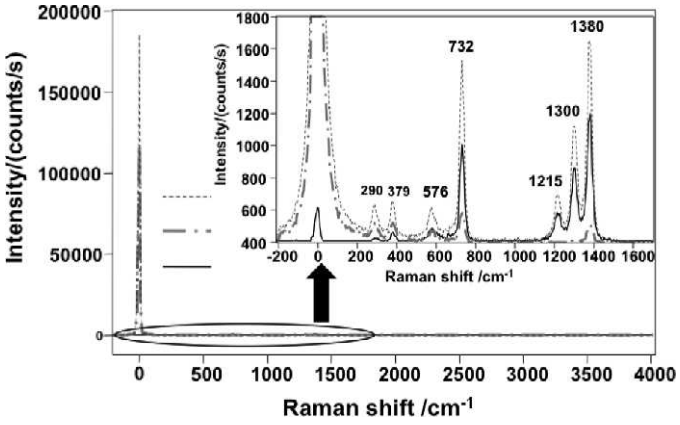

FIG. 6. Teflon 229 nm UV Raman spectra in the absence (- - -) and presence (———) of the CCA filter at an incident glancing angle of ~69°. In addition, the Raman spectrum is shown for the CCA close to normal incidence (— · —). The inset shows an expansion of the circled region.

integrated areas) of the Rayleigh scattered light at 229 nm while transmitting the Raman bands of Teflon including the low-frequency band at 290 cm^{-1} ($\Delta\lambda = 1.5$ nm). At around normal incidence for the CCA, Fig. 6 shows that most of the "Rayleigh peak" is present, while the CCA filter rejects the Raman scattered light at ~1215 cm^{-1} (~236 nm), as expected from Fig. 4.

We calculated the transmissions at the wavelengths of the Teflon Raman bands from the ratios of the integrated Raman band intensities with the CCA filter placed at the incident glancing angle of ~69° to that in the absence of the CCA filter (Fig. 6). These transmission data were plotted against wavelength as shown by the dots in Fig. 7 and compared to the directly measured transmission from the UV-Vis spectrometer. The Raman data indicate that the CCA filter has a higher rejection efficiency (99.82%) and narrower diffraction bandwidth (HWHM: 2 nm) than the measured transmission (Fig. 4). This is because the incident light is well collimated for the CCA filter Raman measurements, while the absorption spectrophotometer uses a somewhat focused beam; the Bragg diffraction strongly depends on the incident angle (Eq. 1). We also directly measured that the CCA filter shows a rejection

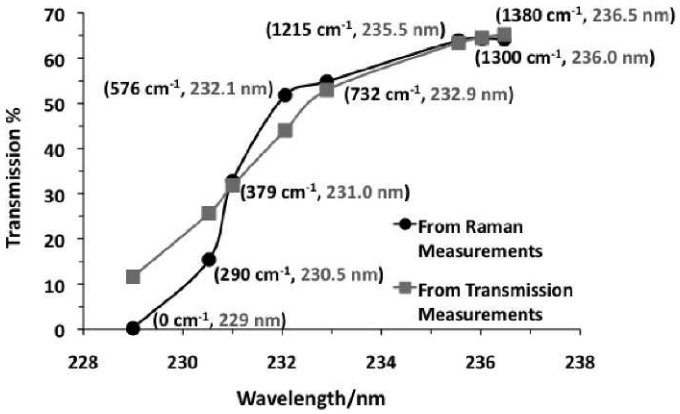

FIG. 7. Transmission calculated from the ratios of integrated intensities of Teflon Raman bands in Fig. 6 for CCA at glancing incident angle of ~69° (black dots). Also shown are transmission data from Fig. 4 for CCA at glancing incident angle of ~69° (grey squares). For comparison, the Raman shifts and corresponding wavelengths are listed next to the data.

efficiency of 99.9% of the incident 229 nm laser beam using a silicon power meter.

CONCLUSIONS

We developed a method to synthesize highly charged, monodisperse silica particles with diameters of ~50 nm as well as distinctly larger diameters. We can easily incorporate surface charge by reacting the silica particles with the sulfonated silating agent THOPS. The highly charged silica particles self assemble into CCAs that Bragg diffract light in the deep UV. The CCA Bragg diffracted wavelength can be tuned from 237 nm to 227 nm by tilting the incident glancing angle from ~90° to ~66°. We also demonstrate that the silica CCA filter can be used as a Rayleigh rejection filter for 229 nm deep UV Raman measurements of highly scattering Teflon. The UV Raman measurements show a Rayleigh rejection efficiency of 99.82% and a narrower bandwidth (HWHM = 2 nm). We expect that the performance of the CCA filter can be improved by increasing the ordering of the CCA FCC array by increasing the particle monodispersity and charge.

ACKNOWLEDGMENTS

The authors acknowledge support for this work from the National Institutes of Health (NIH) grant 1R01EB009089. The authors also thank David Tuschel for the help on Teflon Raman measurements as well as Dr. Dan Qu, Zhenmin Hong, and Lu Ma for many helpful discussions.

1. M. Vieira, M. A. Vieira, P. Louro, J. Costa, M. Fernandes, A. Fantoni, and M. Barata, J. Nanosci. Nanotechnol. **11,** 5299 (2011).
2. Z. Raszewski, E. Kruszelnicki-Nowinowski, J. Kedzierski, P. Perkowski, W. Piecek, R. Dabrowski, P. Morawiak, and K. Ogrodnik, Mol. Cryst. Liquid Cryst. **525,** 112 (2010).
3. J. Lee, C. Hahn, B. Wang, K. Reichard, D. Ditto, D. Glista, Q. Wang, and S. Yin, Opt. Commun. **258,** 184 (2006).
4. J. Philip, T. Jaykumar, P. Kalyanasundaram, and B. Raj, Meas. Sci. Technol. **14,** 1289 (2003).
5. N. Gupta, Methods Mol. Biol. **503,** 293 (2009).
6. S. H. Lim and E. T. Yu, Appl. Phys. Lett. **95,** 161107 (2009).
7. P. L. Flaugh, S. E. O'Donnell, and S. A. Asher, Appl. Spectrosc. **38,** 847 (1984).
8. S. A. Asher and P. L. Flaugh, Spectroscopy **1,** 26 (1986).
9. G. B. Semenov, A. K. Aristov, T. V. Shchedrunova, A. V. Varnaev, A. P. Zhevlakov, and V. M. Grozdilov, J. Opt. Technol. **72,** 196 (2005).
10. B. M. Cullum, J. Mobley, Z. Chi, D. L. Stokes, G. H. Miller, and T. Vo-Dinh, Rev. Sci. Instrum. **71,** 1602 (2000).
11. J. Mobley, B. M. Cullum, A. L. Wintenberg, S. S. Frank, R. A. Maples, D. L. Stokes, and T. Vo-Dinh, Rev. Sci. Instrum. **75,** 2016 (2004).
12. A. E. Fox, K. Rai, and A. K. Fontecchio, Appl. Opt. **46,** 6277 (2007).
13. S. Lebedkin, C. Blum, N. Stürzl, F. Hennrich, and M. M. Kappes, Rev. Sci. Instrum. **82,** 013705 (2011).
14. M. Paillet, F. Meunier, M. Verhaegen, S. Blais-Ouellette, and R. Martel, Rev. Sci. Instrum. **81,** 053111 (2010).
15. S. A. Asher, "Crystalline Colloidal Narrow Band Radiation Filter," U. S. Patent 4,627,689, December 9, 1986.
16. S. A. Asher, "Crystalline Colloidal Narrow Band Radiation Filter," U. S. Patent 4,632,517, December 30, 1986.
17. K. Kang, Y. K. Koh, C. Chiritescu, X. Zheng, and D. G. Cahill, Rev. Sci. Instrum. **79,** 114901 (2008).
18. S. Pilotto, M. T. Pacheco, L. Silveira, A. B. Villaverde, and R. A. Zangaro, Lasers Med. Sci. **16,** 2 (2001).
19. C. J. de Lima, M. T. T. Pacheco, A. B. Villaverde, R. A. Zangaro, L. M. Moreira, and A. J. Damiao, Spectroscopy **22,** 459 (2008).
20. P. Matousek, Appl. Spectrosc. **61,** 845 (2007).
21. C. H. Munro, V. Pajcini, and S. A. Asher, Appl. Spectrosc. **51,** 1722 (1997).
22. M. J. Pelletier, *Analytical Applications of Raman Spectroscopy* (Blackwell Science, Ltd., Oxford, 1999), p. 87.
23. A. C. Greenham, B. A. Nichols, R. M. Wood, N. Nourshargh, and K. L. Lewis, Opt. Eng. **32,** 1018 (1993).
24. M. Zajac and J. Nowak, Appl. Opt. **29,** 5198 (1990).

25. M. J. Pelletier and R. C. Reeder, Appl. Spectrosc. **45,** 765 (1991).
26. B. Yang, M. D. Morris, D. Michael, and H. Owen, Appl. Spectrosc. **45,** 1533 (1991).
27. P. A. Rundquist, P. Photinos, S. Jagnnathan, and S. A. Asher, J. Chem. Phys. 91, 4932 (1989).
28. S. A. Asher, L. Wang, and D. Tuschel, "Crystalline Colloidal Array Deep UV Narrow Band Radiation Filter," U.S.13/227,066, Patent Pending.
29. W. Stöber and A. Fink, J. Colloid Interface Sci. **26,** 62 (1968).
30. M. L. Hair and W. Hertl, J. Phys. Chem. **74,** 91 (1970).
31. Y. Kwon, *Handbook of Essential Pharmacokinetics, Pharmacodynamics, and Drug Metabolism for Industrial Scientists* (Kluwer Academic/Plenum Publishers, New York, 2001), p. 43.
32. C. Beck, W. Hartl, and R. Hempelmann, Angew. Chem. Int. Ed. **38,** 1297 (1999).
33. S. A. Asher, J. Holtz, L. Liu, and Z. Wu, J. Am. Chem. Soc. **116,** 4997 (1994).
34. P. A. Hiltner and I. M. Krieger, J. Phys. Chem. **73,** 2386 (1969).
35. I. M. Krieger and F. M. O'Neill, J. Am. Chem. Soc. **90,** 3114 (1968).
36. G. Pan, A. K. Sood, and S. A. Asher, J. Appl. Phys. **84,** 83 (1998).
37. A. Tikhonov, R. D. Coalson, and S. A. Asher, Phys. Rev. B **77,** 235404 (2008).
38. S. A. Asher, J. M. Weissman, A. Tikhonov, R. D. Coalson, and R. Kesavamoorthy, Phys. Rev. E **69,** 066619 (2004).
39. P. Yeh, A. Yariv, and C. S. Hong, J. Opt. Soc. Am. **67,** 423 (1977).